Selective Synthesis of Monazite- and Zircon-type $LaVO_4$ Nanocrystals

Chun-Jiang Jia,[†] Ling-Dong Sun,*[,†] Li-Ping You,[‡] Xiao-Cheng Jiang,[†] Feng Luo,[†] Yu-Cheng Pang,[†] and Chun-Hua Yan*[,†]

State Key Lab of Rare Earth Materials Chemistry and Applications and PKU−HKU Joint Lab in Rare Earth Materials and Bioinorganic Chemistry, Peking University, Beijing 100871, China, and Electron Microscopy Laboratory, Peking University, Beijing 100871, China

Received: September 7, 2004; In Final Form: October 23, 2004

Pure monoclinic (*m*-) and tetragonal phased (*t*-) $LaVO_4$ nanocrystals could be obtained by a hydrothermal method in a controllable way with additives. It is found that chelating ligands, such as ethylenediaminetetraacetic acid [EDTA or H_4L, where $L^{4-} = (CH_2COO)_2N(CH_2)_2N(CH_2COO)_2^{4-}$], favor the formation of *t*-$LaVO_4$ and can induce the polymorph transformation from stable *m*-$LaVO_4$ to metastable *t*-$LaVO_4$. Further studies demonstrated the important roles of chelating ligands in this transformation process. Careful investigation over the phase transition from *t*- to *m*-$LaVO_4$ was also conducted with high-temperature X-ray diffraction (HTXRD) studies. The phase transition occurred at 850 °C, which is about 250 °C higher than for the bulk. The enhanced thermal stability of the nanosized metastable *t*-$LaVO_4$ may come from the small size effect. Our capability of obtaining and stabilizing *t*-$LaVO_4$ not only benefits the wider applications based on $LaVO_4$ due to the improved luminescent and catalytic performance but also provides a new idea in the studies of polymorph control and selective synthesis of inorganic materials.

Introduction

Selective synthesis of desirable phased inorganic materials has attracted great interest due to its significance in synthetic chemistry, crystal engineering, and practical applications.[1−6] Especially, intrigued by the novel properties of some metastable phased materials, more research is involved in the exploration of polymorph selection in recent years. Furthermore, the acquirement and stabilization of metastable phases[7,8] with desirable properties are currently among the most challenging objectives in solid-state science.

Lanthanide orthovanadates are an important rare earth compound family due to their wide applications as catalysts,[9] polarizers,[10] laser host materials,[11] and phosphors.[12] Lanthanide orthovanadates crystallize in two polymorphs, that is, tetragonal phase (*t*) with zircon structure and monoclinic phase (*m*) with monazite structure. Generally, with increasing ionic radius, Ln^{3+} ions show a strong tendency toward monazite-structured orthovanadate due to its higher oxygen coordination number of 9 as compared with 8 of the zircon one. For this reason $LaVO_4$ chooses monazite type as the thermodynamically stable state while the other orthovanadates normally exist in the zircon type. Determined by its structural characteristics, *m*-$LaVO_4$ [$C_{2h}^5 P2_1/n$, $a = 7.0434(5)$ Å, $b = 7.2793(7)$ Å, $c = 6.7211(6)$ Å] is neither a suitable host for luminescent activators[13,14] nor a promising catalyst[9] compared to other orthovanadates. On the contrary, *t*-$LaVO_4$ [$D_{4h}^{19} I4_1/amd$, $a = b = 7.4578(7)$ Å, $c = 6.5417(9)$ Å] is expected to possess superior properties, as revealed by our preliminary research.[15] As a result, the selective synthesis of *m*- and *t*-$LaVO_4$ not only has great theoretical significance in studying the polymorph conversion/phase transition processes and the structure-dependent properties but also is very important for their potential applications.

Generally, thermodynamically stable *m*-$LaVO_4$ can be obtained by conventional solid-state reaction.[16] For *t*-$LaVO_4$, the metastable phased material, it can only be prepared through solution process. Ropp and Carroll[17] first reported the synthesis of *t*-$LaVO_4$ and obtained a low crystallinity product. Thereafter, Escobar and Baran[18] also obtained *t*-$LaVO_4$ by mixing NH_4VO_3 and $La(NO_3)_3$ solution at 50−60 °C. However, Chakoumakos et al.[19] claimed that they failed to reproduce zircon-type $LaVO_4$ by following the method in ref 18. Oka et al.[20] reported the synthesis of *t*-$LaVO_4$ single crystal by a hydrothermal method and pointed out that lanthanum and vanadium sources affected the polymorphs of La−V−O. On the basis of the report by Oka, regardless of the V sources including V_2O_5, $VO(OH)_2$, and Na_3VO_3, $La(NO_3)_3$ always produced *m*-$LaVO_4$. Investigations on the crystallization and crystal growth process in a controllable and reproducible way toward expected structured materials are essential for not only $LaVO_4$ but also other functional materials. Our preliminary results[15] showed that *t*-$LaVO_4$ can be reproducibly obtained with $La(NO_3)_3$ and Na_3VO_4 as starting materials by an ethylenediaminetetraacetic acid [EDTA or H_4L, where $L^{4-} = (CH_2COO)_2N(CH_2)_2N(CH_2COO)_2^{4-}$] mediated hydrothermal method. In this case, besides the V and La sources, organic molecules additives play an important role in the polymorph selection of $LaVO_4$ system. The additive-mediated hydrothermal method provides a new approach to synthesize metastable *t*-$LaVO_4$.

In recent years, much attention has been paid to the synthesis of nanoscale materials due to their interesting properties and potential applications. Despite numerous reports about the synthesis and property studies of nanoscale lanthanide orthovanadate materials,[21−29] systematic studies over controllable synthesis and properties of both *m*- and *t*-$LaVO_4$ nanocrystals are limited. In this paper, *m*- and *t*-$LaVO_4$ nanocrystals with

* Corresponding authors: fax +86-10-6275-4179; e-mail yan@pku.edu.cn.
† State Key Lab of Rare Earth Materials Chemistry and Applications and PKU−HKU Joint Lab in Rare Earth Materials and Bioinorganic Chemistry.
‡ Electron Microscopy Laboratory.

10.1021/jp045967u CCC: $30.25
Published on Web 02/05/2005

high crystallinity were successfully synthesized by a hydrothermal method. It is found that chelating ligands, such as EDTA, favor the formation of *t*-$LaVO_4$ and can induce the transformation of $LaVO_4$ nanocrystals from monazite to zircon type. This chelating ligand-mediated hydrothermal method is prominent in polymorph selection, and the resulting improvement in thermal stability, luminescence, and catalytic performance is believed to greatly broaden the applications of $LaVO_4$.

Experimental Section

1. Preparations. In the preparation procedure, 0.0016 mol of $La(NO_3)_3$ aqueous solution [dissolved from La_2O_3 (>99.99%)], 0.0016 mol of $Na_3VO_4 \cdot 12H_2O$ (0.640 g), appropriate amount of additives such as acetic sodium, citric sodium, $Na_2H_2L \cdot 2H_2O$, DTPA (diethylenetriaminepentaacetic acid), CyDTA (*trans*-1: 2-diaminocyclohexanetetraacetic acid), and some distilled water were mixed with vigorous stirring. The pH value of the mixture was adjusted from 2 to 13 by the addition of 3 M HNO_3 or NaOH solution, and the final volume of the mixture was kept as 80 mL. After stirring for 10 min, the mixture was transferred into a Teflon-lined stainless steel autoclave with a capacity of 100 mL for hydrothermal treatment at 120−240 °C for 0.5−24 h. As the autoclave cooled to room temperature naturally, the precipitation was separated by centrifugation, washed with distilled water and absolute ethanol, and dried under vacuum at 80 °C.

Eu^{3+} ion-doped $LaVO_4$ nanocrystals are prepared by introducing the proper amount of $Eu(NO_3)_3$ to the precursor mixture as described above. The same hydrothermal treatment was conducted. To obtain the pure *m*-$LaVO_4$−Eu (5%) nanocrystals, citric sodium ([citric acid]:[La^{3+}, Eu^{3+}] = 3:1) was added to suppress the phase separation. *t*-$LaVO_4$−Eu (5%) nanocrystals are prepared by a similar route except for replacing citric sodium with $Na_2H_2L \cdot 2H_2O$ ([$H_xL^{(4-x)-}$]/[La^{3+}, Eu^{3+}] = 1/12).

2. Characterizations. The powder X-ray diffraction (XRD) patterns were recorded on a Rigaku D/max-2000 diffractometer with Cu Kα radiation (λ = 1.5418 Å). Vis−Raman spectra were determined on a Renishaw (U.K.) spectrometer with an Ar ion laser of 514.5 nm as excitation source. Backscattering geometry was adopted for the measurement with a laser power of 20 mW and a resolution of 4 cm^{-1}. Transmission electron microscopic (TEM) images were taken on a JEOL 200CX transmission electron microscope under a working voltage of 160 kV. High-resolution TEM (HRTEM) characterizations were performed with a Philips Tecnai F30 FEG-TEM operated at 300 kV. The Eu content of $LaVO_4$−Eu nanocrystals was determined by energy-dispersive X-ray analysis (EDAX) on the Hitachi H-9000 NAR TEM under a working voltage of 300 kV. The samples were supported on carbon-coated copper grids by dropping the ethanol suspension containing uniformly dispersed samples. High-temperature powder X-ray diffraction (HTXRD) patterns of the as-prepared nanocrystals were recorded on a Bruker D8 Advance powder X-ray diffractometer equipped with a scanning position-sensitive detector (PSD), employing Cu $K\alpha_1$ radiation (λ = 1.5406 Å). Data were collected in step-scanning mode with a step of $2\theta = 0.0144°$ and dwell time of 1 s at each step between 10° and 80°. The samples were heated to 900 °C on the surface of the Pt strip in air with a speed of 0.2 °C s^{-1} and cooled at the same rate to room temperature. Data were recorded from room temperature with intervals of 50 °C and dwell time of 10 min at each step. Fluorescence spectra were recorded on a Hitachi F-4500 spectrophotometer equipped with a 150 W Xe arc lamp at room temperature; the emission spectra were measured at a fixed band-pass of 0.2 nm with the same instrument parameters (5.0 nm for excitation split, 1.0 nm for emission split, and 700 V for PMT voltage). The BET surface areas of the samples were measured by N_2 adsorption on an ASAP 2010 analyzer. The catalytic evaluation was performed at 500 °C in a fixed-bed quartz microreactor in a flow system (C_3H_8:O_2 = 2:1). The reaction products were analyzed with an on-line Varian CP3800 gas chromatograph.

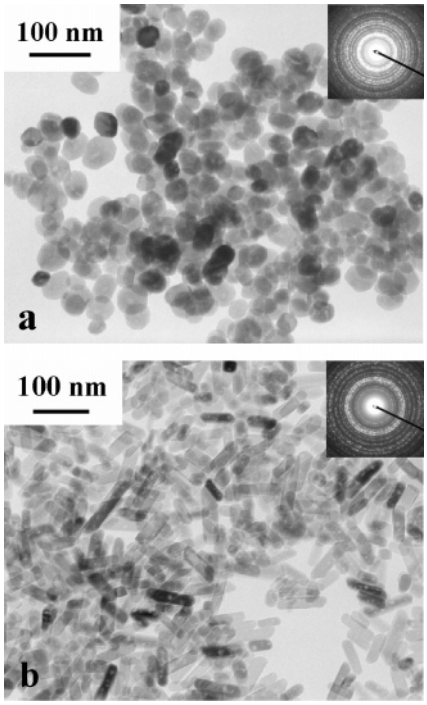

Figure 1. TEM images of *m*-$LaVO_4$ nanocrystals.

Results and Discussion

1. Synthesis of *m*-$LaVO_4$ Nanocrystals. Monazite-type $LaVO_4$ can be obtained in a wide pH range (from 2 to 13) by choosing $La(NO_3)_3$ and Na_3VO_4 solution as starting material through hydrothermal treatment. TEM images of the *m*-$LaVO_4$ nanocrystals obtained at 210 °C for 24 h are shown in Figure 1. Uniform particles with diameters from 20 to 50 nm were obtained when the pH is 5 or 6 (Figure 1a). As the pH value ranged from 7 to 13, the as-obtained *m*-$LaVO_4$ nanocrystals exhibited rodlike morphology with diameter of 20 nm and length from 50 to 100 nm (Figure 1b). When the pH value was lower than 4, larger submicrometer-sized crystals appeared. When the reaction temperature was varied from 120 to 240 °C, similar results were obtained. The formation of two different sized and shaped *m*-$LaVO_4$ crystals may be due to the different crystallization style of lanthanide orthovanadates in acidic and basic media.[29] The morphology division at different pH may come from the status of rare earth ions and their hydroxy form. Under higher pH conditions the morphology of $LaVO_4$ is mainly determined by the shape of the relevant rare earth hydroxide, which is one-dimensional under hydrothermal treatment. The XRD patterns of the *m*-$LaVO_4$ nanocrystals obtained at pH 6 and 12 at 210 °C are shown in Figure 2. All the diffraction peaks are well indexed to the *m*-$LaVO_4$ (JCPDS 50-0367), and no traces of other phases are examined. It is understandable that $LaVO_4$ crystallizes in its thermodynamic state, the monazite structure.

For the spherelike particles, the crystalline domain calculated from the XRD patterns was 30.9 nm, which is in accordance with the TEM observations (Figure 1a). But for the one-

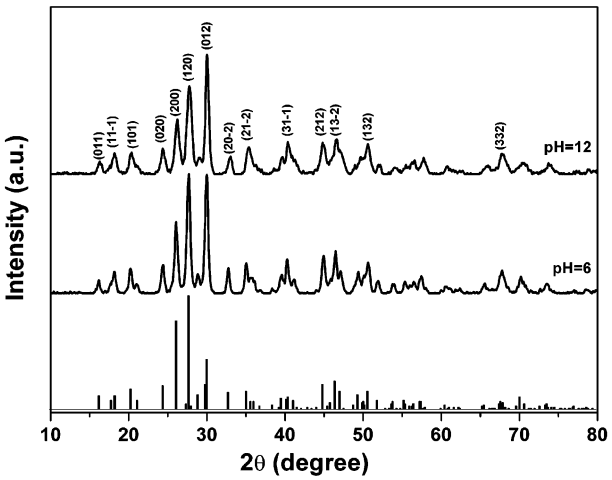

Figure 2. XRD patterns of *m*-$LaVO_4$ nanocrystals.

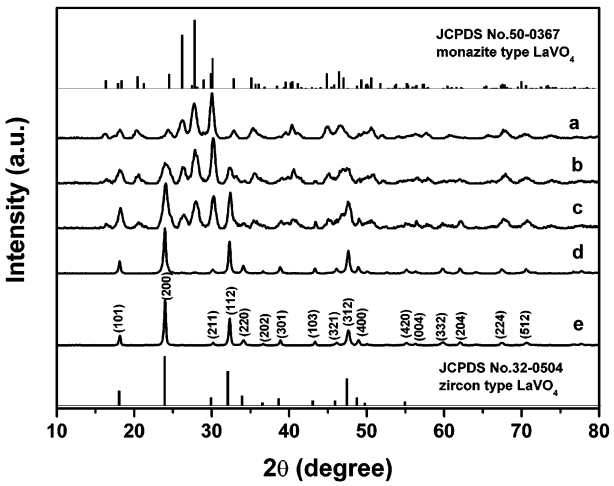

Figure 3. XRD patterns of $LaVO_4$ nanocrystals (a) without $Na_2H_2L\cdot 2H_2O$ and with (b) 0.010 g of $Na_2H_2L\cdot 2H_2O$ ($[H_xL^{(4-x)-}]/[La^{3+}] = 1/60$), (c) 0.020 g of $Na_2H_2L\cdot 2H_2O$ ($[H_xL^{(4-x)-}]/[La^{3+}] = 1/30$), (d) 0.030 g of $Na_2H_2L\cdot 2H_2O$ ($[H_xL^{(4-x)-}]/[La^{3+}] = 1/20$), and (e) 0.050 g of $Na_2H_2L\cdot 2H_2O$ ($[H_xL^{(4-x)-}]/[La^{3+}] = 1/12$). Standard XRD patterns of JCPDS 50-0367 and 32-0504 are also shown.

dimensional particles that seriously deviated from the sphere, it is hard to get size information on either diameter or length just from XRD patterns. An accurate crystalline domain should be obtained from direct observations. The electronic diffraction (ED) patterns (inset of Figure 1) composed of bright spots indicated the high crystallinity of the *m*-$LaVO_4$ nanocrystals prepared by the hydrothermal method.

2. Zircon-type $LaVO_4$ Nanocrystals: Synthesis and Thermal Stability. As shown in the former part, zircon-type $LaVO_4$ cannot be obtained through direct hydrothermal treatment of the mixture of $La(NO_3)_3$ and Na_3VO_4 solution. Additives have long been recognized as an efficient means to adjust the morphology and uniformity of products in the crystallization process.[30−34] Similarly, our research revealed that some additives could also modulate the phase of the products. Several conventional ligands including acetic acid, citric acid, and EDTA were introduced into the reaction system to mediate the growth of $LaVO_4$. The results show that weak ligands such as sodium acetate and sodium citrate have little effect on the polymorph selection of *m*-$LaVO_4$ but can apparently promote the crystallization. Compared with weak ligands, chelating ligands, such as EDTA, favor the formation of zircon-structured $LaVO_4$ nanocrystals instead of monazite one. What is more, the transformation of $LaVO_4$ from monazite to zircon type is quite controllable, as will be discussed below.

By modulating the amount of $Na_2H_2L\cdot 2H_2O$ with the fixed pH value of 10 (at this pH value, the coordination ability between La^{3+} and $H_xL^{(4-x)-}$ ($0 \le x < 1$) is the strongest), we investigated the formation process of *t*-$LaVO_4$ and the effect of EDTA. The XRD patterns of the products that were hydrothermally treated at 210 °C for 24 h with different amount of $Na_2H_2L\cdot 2H_2O$ (ratios of $[H_xL^{(4-x)-}]/[La^{3+}]$ are 0, 1/60, 1/30, 1/20, and 1/12) are shown in Figure 3. Without $Na_2H_2L\cdot 2H_2O$, pure *m*-$LaVO_4$ is obtained (Figure 3a). When $Na_2H_2L\cdot 2H_2O$ is added, the formation of *m*-$LaVO_4$ is evidently restrained and the peaks of *t*-$LaVO_4$ appeared. Obviously, the increase of the amount of $Na_2H_2L\cdot 2H_2O$ put forward the formation of *t*-$LaVO_4$. When 0.05 g of $Na_2H_2L\cdot 2H_2O$ is added ($[H_xL^{(4-x)-}]/[La^{3+}] = 1/12$), pure *t*-$LaVO_4$ can be obtained (Figure 3e). It is evident that EDTA, with the distinct phenomenon of favoring the formation of *t*-$LaVO_4$, can be used as a very efficient phase regulator.

The Raman spectra (Figure 4) also clearly demonstrate that EDTA favors the formation of *t*-$LaVO_4$. The spectra are composed of two parts: namely, one is the high-energy part between 745 and 880 cm^{-1}, which corresponds to the "internal"

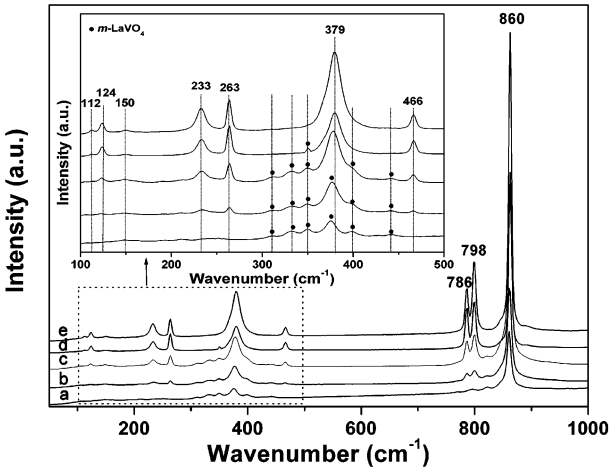

Figure 4. Raman spectra of as-obtained $LaVO_4$ nanocrystals (the inset is an enlargement of the part from 100 to 500 cm^{-1}) (a) without $Na_2H_2L\cdot 2H_2O$ and with (b) 0.010 g of $Na_2H_2L\cdot 2H_2O$ ($[H_xL^{(4-x)-}]/[La^{3+}] = 1/60$), (c) 0.020 g of $Na_2H_2L\cdot 2H_2O$ ($[H_xL^{(4-x)-}]/[La^{3+}] = 1/30$), (d) 0.030 g of $Na_2H_2L\cdot 2H_2O$ ($[H_xL^{(4-x)-}]/[La^{3+}] = 1/20$), and (e) 0.050 g of $Na_2H_2L\cdot 2H_2O$ ($[H_xL^{(4-x)-}]/[La^{3+}] = 1/12$).

vibrations of the tetrahedral VO_4 group, and the other is the vibrations below 475 cm^{-1}, which mainly originates from the La−O vibrations. With increasing amounts of $Na_2H_2L\cdot 2H_2O$, the monoclinic phase of $LaVO_4$ gradually disappears and tetragonal phase forms. Because of the structure difference between *m*- and *t*-$LaVO_4$, the Raman spectra, especially the low-energy region (as shown in the inset of Figure 4) that corresponds to the La−O vibrations below 475 cm^{-1}, are quite different. The decreased number of vibration peaks for *t*-$LaVO_4$ is in accordance with the lower coordination number (8) and the high symmetry (D_{2d}) of the La^{3+} ions, both of which contribute to the relatively simple vibration spectra compared with that of *m*-$LaVO_4$.

Figure 5 shows the TEM and HRTEM images of as-prepared *t*-$LaVO_4$ nanocrystals. From the TEM and HRTEM images of *t*-$LaVO_4$ prepared with the ratio of $[H_xL^{(4-x)-}]/[La^{3+}]$ as 1/12 (Figure 5a,b) and 1.25 (Figure 5c,d), we can see that *t*-$LaVO_4$ has an obvious anisotropic growth habit. When the ratio of $[H_xL^{(4-x)-}]/[La^{3+}] < 1$, small rodlike nanocrystals are obtained.

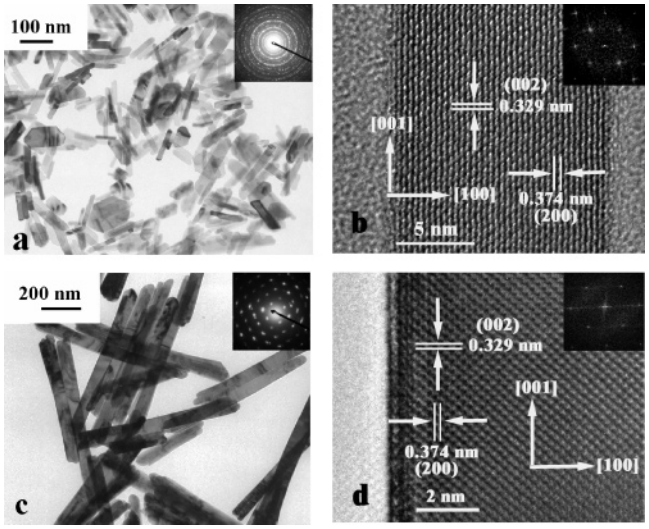

Figure 5. TEM and HRTEM images of as-obtained *t*-$LaVO_4$ nanocrystals ($[H_xL^{(4-x)-}]/[La^{3+}] = 1/12$) (a and b) and *t*-$LaVO_4$ nanorods ($[H_xL^{(4-x)-}]/[La^{3+}] = 1.25/1$) (c and d).

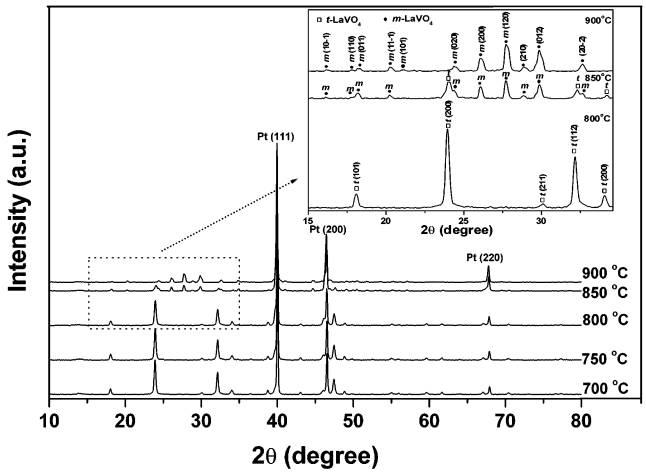

Figure 6. HTXRD patterns of as-obtained *t*-$LaVO_4$ nanocrystals (the inset is an enlargement of the part from 15° to 35°).

And when $[H_xL^{(4-x)-}]/[La^{3+}] \geq 1$, uniform nanorods can be obtained. The clear lattice fringes in the HRTEM images confirm the high crystallinity of as-prepared *t*-$LaVO_4$ nanocrystals. The deduced growth direction of the nanorods is [001], parallel to the *c*-axis. The preferential growth mediated by EDTA may be ascribed to the mediating effect of EDTA, as discussed for the $BaSO_4$ system.[34]

t-$LaVO_4$ is in a metastable state, which is reported to transform into *m*-$LaVO_4$ below 600 °C.[17−19] To investigate the phase transition behavior of as-prepared *t*-$LaVO_4$ nanocrystals (corresponding to Figure 5a), HTXRD diffractograms were recorded as the samples were in situ heated to 900 °C and then cooled to room temperature. Figure 6 shows the HTXRD patterns recorded for the as-prepared *t*-$LaVO_4$ nanocrystals. It is noted that the sample keeps the phase of pure tetragonal structure till 800 °C. At 850 °C, the peaks of *m*-$LaVO_4$ appeared, while *t*-$LaVO_4$ diminished prominently. As the temperature reached 900 °C, the tetragonal phase completely disappeared. This suggests that the *t* to *m* transformation occurs at ca. 850 °C and finishes at ca. 900 °C. As the temperatures rose higher than 900 °C, the samples sustained the monoclinic structure. Compared to the data in the literature,[17−19] the thermal stability of the *t*-$LaVO_4$ nanocrystals is greatly improved, which may come from the small size effect to suppress the phase transition

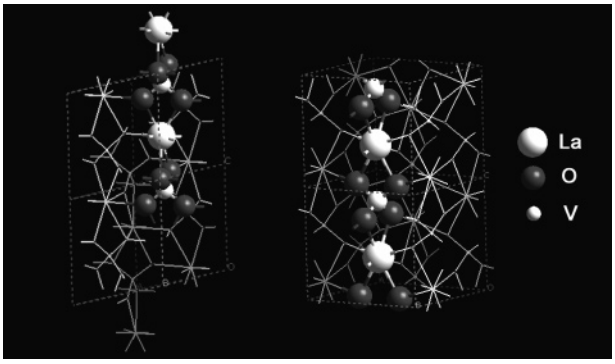

Figure 7. Simulated crystal structures of *m*-$LaVO_4$ (left) and *t*-$LaVO_4$ (right).

like zirconia,[35] alumina,[36] and graphite[37] systems. The improved thermal stability offers a wider temperature range to study the properties of *t*-$LaVO_4$.

3. Effect of Chelating Ligands on the Formation of *t*-$LaVO_4$. Additives as phase regulators have been observed in several systems;[38−41] however, polymorph transformation from stable to metastable state induced by certain molecules is rarely reported. In the following section, we will make careful exploration of this distinguished phenomenon.

The key point to our comprehension of the transformation process lies in the explanation of the preference of EDTA for the metastable *t*-$LaVO_4$. It is reported that the adsorption of additives on certain crystal surfaces plays a crucial role in the polymorph selection for some materials.[38−40] However, for the formation of *t*-$LaVO_4$, the existence of LaL^- [where $L^{4-} = (CH_2COO)_2N(CH_2)_2N(CH_2COO)_2^{4-}$] ought to be the key factor that induces the transformation from *m*- to *t*-$LaVO_4$. A rigid physical derivation is somewhat difficult for this complex system, but we could still get some convincing conclusions by carefully analyzing the crystal structures of these two competitive products, *m*- and *t*-$LaVO_4$ (Figure 7). Generally, La^{3+} ion prefers a high coordination number of 9 because of its large radius, which could be satisfied in the *m*-$LaVO_4$ (for *t*-$LaVO_4$, the coordination number of La^{3+} ion is 8); this is why $LaVO_4$ tends to crystallize in the *m*-phase normally. With the existence of Na_2H_2L, LaL^- forms due to the strong chelating interactions between La^{3+} ions and $H_xL^{(4-x)-}$. In this case, L^{4-} occupies most of the coordination sites of La^{3+} and "protects" it efficiently. The strong steric hindrance of L^{4-} and repulsion between coordinating atoms forced $LaVO_4$ to crystallize in a manner with fewer coordination number. As a result, the formation of *t*-$LaVO_4$ is preferred with the assistance of EDTA. In this process, EDTA chelated with La^{3+} and functioned as a "block". This means EDTA should not be the only candidate for phase regulation. In fact, our experiments have shown that other chelating ligands, such as DTPA and CyDTA, possess similar functions. On the contrary, ligands such as acetic or citric acid do not show such effects. Their weaker bonding with La^{3+} ions induces a higher proportion of dissociation at high temperature, thus imposing less steric hindrance in the crystallization process.

Besides the effect of EDTA, other factors such as reaction time, temperature, and pH value can also directly affect the formation of *t*-$LaVO_4$. To have a complete view of the formation process of *t*-$LaVO_4$ with the mediation of EDTA, the polymorph selection behaviors of $LaVO_4$ at different conditions were also carefully investigated.

Figure 8A(b−f) shows the XRD patterns of the products obtained for different times of hydrothermal treatment with a

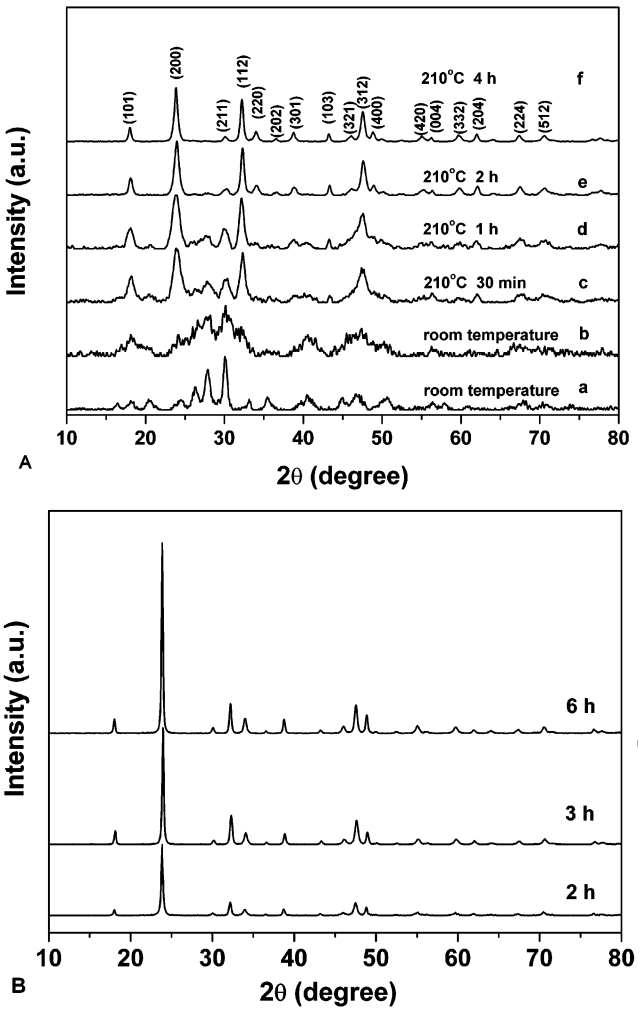

Figure 8. XRD patterns of $LaVO_4$ nanocrystals obtained for different reaction times. (A) (a) Without EDTA at room temperature; (b−f) $[H_xL^{(4-x)-}]/[La^{3+}] = 1/12$. (B) $[H_xL^{(4-x)-}]/[La^{3+}] = 1.25/1$.

lower ratio of $[H_xL^{(4-x)-}]/[La^{3+}]$, 1/12. In comparison, the XRD patterns of the $LaVO_4$ obtained by directly mixing La^{3+} and VO_4^{3-} with the pH value of 10 at room temperature for 2 h are also shown in Figure 8A(a). It is obvious that *m*-$LaVO_4$ [see Figure 8A(a)] formed at room temperature without any additives. With the existence of EDTA, however, the formation of *m*-$LaVO_4$ was restrained and the traces of *t*-$LaVO_4$ appeared, as can be seen from Figure 8A(b). When the above product was further hydrothermally treated, we can see that *m*-$LaVO_4$ gradually vanished and *t*-$LaVO_4$ become dominant. With prolonged treatment to 4 h, pure *t*-$LaVO_4$ was obtained [Figure 8A(f)]. It is clear and prominent that a small amount of EDTA can drive the transformation of $LaVO_4$ from monoclinic to tetragonal phase under hydrothermal treatment. Additionally, the formation of *t*-$LaVO_4$ with higher ratio of $[H_xL^{(4-x)-}]/[La^{3+}]$ (1.25) is also examined. Because of the strong chelating ability of EDTA, when La^{3+}, VO_4^{3-}, and Na_2H_2L were mixed, only a clear solution was formed. Even when the solution was hydrothermally treated for 1.5 h, no precipitates appeared. But the TEM observations indicated that small particles (<10 nm) already formed. With further hydrothermal treatment for over 2 h, white precipitates are obtained, and the XRD patterns (Figure 8B) indicate the high phase purity of *t*-$LaVO_4$. Our results show that only when the ratio of $[H_xL^{(4-x)-}]/[La^{3+}]$ is larger than 1 can *t*-$LaVO_4$ form directly.

On the basis of the facts above, we could then have a complete view of the transformation process form *m*- to *t*-$LaVO_4$, which is shown in Scheme 1. If the ratio of $[H_xL^{(4-x)-}]/[La^{3+}]$ is low, for example, 1/12, *m*-$LaVO_4$ forms as the direct precipitate (eq 1). At the same time, those EDTA-chelated La^{3+} ions (eq 2) precipitate as *t*-$LaVO_4$, which is shown in eq 3.

SCHEME 1: Formation Process of *t*-$LaVO_4$ Nanocrystals[a]

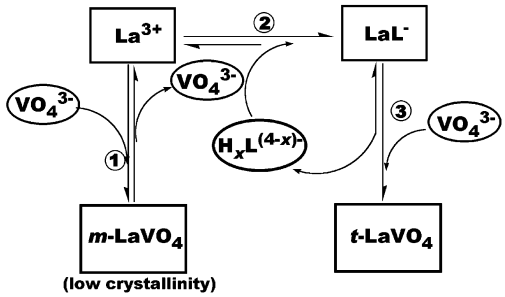

[a] Reaction routes 1, 2, and 3 represent eqs 1, 2, and 3, respectively.

$$La^{3+} + VO_4^{3-} \leftrightarrow m\text{-}LaVO_4 \quad (1)$$

$$La^{3+} + H_xL^{(4-x)-} \leftrightarrow LaL^- + xH^+ \quad (2)$$

$$LaL^- + VO_4^{3-} + xH^+ \leftrightarrow t\text{-}LaVO_4 + H_xL^{(4-x)-} \quad (3)$$

As *t*-$LaVO_4$ gradually formed, $H_xL^{(4-x)-}$ ions were released and they kept on putting forward the conversion of more *m*-$LaVO_4$ to *t*-$LaVO_4$ through the dissolution of *m*-$LaVO_4$. The repetition of this process finally leads to the complete transformation of *m*-$LaVO_4$ to *t*-$LaVO_4$. This could explain why only a small amount of EDTA is needed for driving the entire transition. The polymorph conversion of $LaVO_4$ from stable monazite to metastable zircon type is an EDTA-mediated transformation process in solution,[42,43] which is different from the normal transition from unstable to stable state. The existence of EDTA played an important role in this inverse process. If the ratio of $[H_xL^{(4-x)-}]/[La^{3+}]$ is high (≥1), almost all the La species exist as EDTA-chelated La^{3+} ions, and it is impossible for *m*-$LaVO_4$ to form. In the end, *t*-$LaVO_4$ directly formed from EDTA-chelated La^{3+} ion sources.

Practically, however, we should note that for a complete conversion of *m*-$LaVO_4$ to *t*-$LaVO_4$, a minimum amount of Na_2H_2L ($[H_xL^{(4-x)-}]/[La^{3+}] = 1/12$) should be satisfied at the initial stage. Our results show that once *m*-$LaVO_4$ with high crystallinity forms, the transformation to *t*-$LaVO_4$ cannot proceed even with prolonged reaction time and large amounts of Na_2H_2L. When the amount of Na_2H_2L is below this limit, the dissolution of *m*-$LaVO_4$ and the formation of *t*-$LaVO_4$ are greatly decelerated, allowing for an extended crystallization time that leads to the formation of highly crystallized *m*-$LaVO_4$. In this case, only a mixture of *m*- and *t*-$LaVO_4$ can be obtained after a long time (≥24 h) treatment, as indicated in Figure 1b−d. Even if a large amount of Na_2H_2L is added to the freshly prepared high-crystallinity *m*-$LaVO_4$ and hydrothermally treated at 210 °C for 24 h, the product is still pure *m*-$LaVO_4$. So the transformation from *m*- to *t*-$LaVO_4$ can be realized only before highly crystallized *m*-$LaVO_4$ forms.

In a wide pH and temperature range, the effect of EDTA ($[H_xL^{(4-x)-}]/[La^{3+}] = 1/12$) on the polymorph selection behavior of $LaVO_4$ was also investigated. Table 1 shows polymorphs of as-prepared products under different conditions. The XRD patterns of these products are shown in Supporting Information (Figures S1 and S2). It is found that lower temperature (120

TABLE 1: Polymorphs of the $LaVO_4$ Products vs. Reaction Conditions

polymorph	$H_xL^{(4-x)-}/La^{3+}$	pH	temperature (°C)
monazite/zircon	1/12	10	120
zircon	1/12	10	150
zircon	1/12	10	180
zircon	1/12	10	210
zircon	1/12	10	240
monazite	1/12	3	180
monazite	1/12	5	180
monazite/zircon	1/12	6	180
zircon	1/12	7	180
zircon	1/12	9	180
zircon	1/12	10	180
monazite/zircon	1/12	11	180
monazite/zircon	1/12	12	180
monazite/zircon	1/12	13	180

°C) is not beneficial for the transformation from *m*- to *t*-$LaVO_4$, which mainly originates from the lack of enough energy to speed up the dissolution, renucleation, and crystallization process. Furthermore, pH is a critical factor for the formation of $LaVO_4$. The formation of pure *t*-$LaVO_4$ is favored only within the pH range from 7 to 10. Beyond this range, *m*-$LaVO_4$ or mixtures of *m*- and *t*-$LaVO_4$ were obtained. In acidic aqueous media, EDTA species exists in the acid form instead of anion, with weakened coordination ability, and blocks the formation of *t*-$LaVO_4$. In basic media when pH > 10, the combination of La^{3+} and L^{4-} is also weakened due to the strong interaction between La^{3+} and OH^-, which may be the main reason that pure *t*-$LaVO_4$ cannot form.

It is quite interesting that larger crystals are obtained with increasing amounts of EDTA. Besides the polymorph elective effect to put forward the phase tranformation from *m*- to *t*-$LaVO_4$ or induce the formation of *t*-$LaVO_4$, EDTA was also crucial to affect the crystal growth. With a high EDTA/La ratio, both the nucleation and growth processes would be suppressed, but for our system, which is dominated by the Ostwald-ripening process, the impact on nucleation is more important, which greatly decreased the number of nuclei and resulted in large particle size.

4. Luminescence and Catalytic Performances. Despite the fact that rare earth activator-doped vanadates of Y, Gd, and Lu have attracted great interest in view of luminescent applications,[13] $LaVO_4$ is not regarded as a suitable host for rare earth activators due to its ordinary monazite structure.[13,14] However, our preliminary results showed that *t*-$LaVO_4$−Eu, with zircon structure, is also a promising candidate for red phosphor. Here *m*- and *t*-$LaVO_4$−Eu (5%) nanocrystals are obtained by the hydrothermal method with the existence of sodium citrate ([citric acid]:[La^{3+}, Eu^{3+}] = 3:1) or $Na_2H_2L{\cdot}2H_2O$ ([$H_xL^{(4-x)-}$]/[La^{3+}, Eu^{3+}]) = 1/12) at 180 °C for 24 h, respectively. The energy-dispersive X-ray analysis (EDAX) for *m*- and *t*-$LaVO_4$−Eu nanocrystals indicated that the Eu content is 5%. Figure 9 showed the emission spectra of as-prepared *m*- and *t*-$LaVO_4$−Eu nanocrystals excited at 310 nm. The emission intensity of the *t*-$LaVO_4$−Eu nanocrystals is much higher than that of the monazite one and is comparable to that of the commercial Y_2O_3−Eu (5%) phosphor (see Figure S3). The structurally induced luminescence enhancement for $LaVO_4$−Eu mainly arises from the change of the symmetry of host and lattice site of Eu^{3+}, which has been discussed in the literature.[44,45]

As a kind of important inorganic functional material, lanthanide orthovanadates are also widely used as catalysts for the oxidative dehydrogenation of propane (ODP) to propene. But in the case of *m*-$LaVO_4$, it is an unstable active phase that cannot stabilize the surface active sites, which are oxygen vacancies

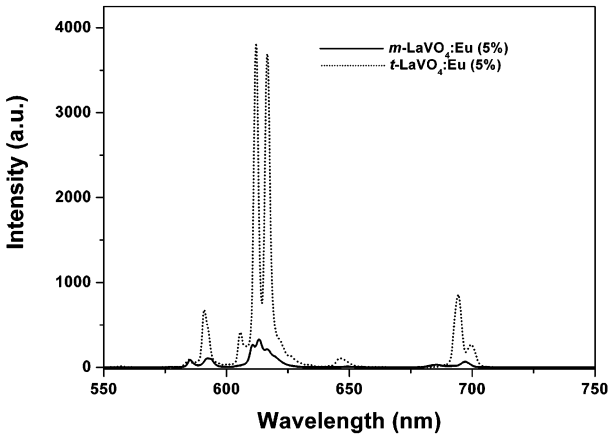

Figure 9. Luminescence spectra of *m*- and *t*-$LaVO_4$−Eu nanocrystals (5%) excited at 310 nm.

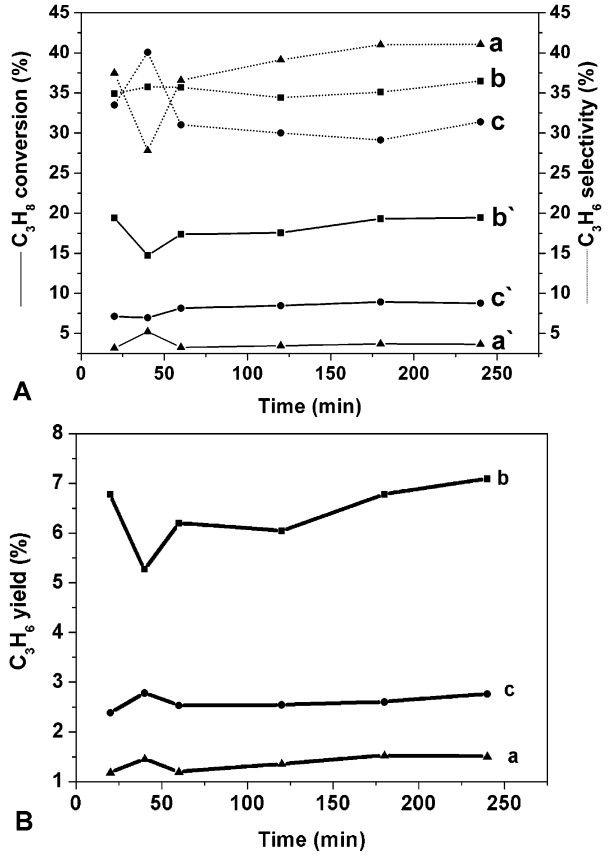

Figure 10. Catalytic performance for ODP to propene. (A) C_3H_6 selectivity (a−c) and conversion (a′−c′) behavior of (a, a′) *m*-$LaVO_4$ nanoparticles, (b, b′) *t*-$LaVO_4$ nanocrystals, and (c, c′) *t*-$LaVO_4$ nanorods. (B) C_3H_6 yield catalyzed by (a) *m*-$LaVO_4$ nanoparticles, (b) *t*-$LaVO_4$ nanocrystals, and (c) *t*-$LaVO_4$ nanorods.

associated with V^{4+} ions. Therefore *m*-$LaVO_4$ is not regarded as a good candidate.[9] The catalytic performances of both *m*- (as indicated in Figure 1a, noted as sample a) and *t*-$LaVO_4$ (as indicated in Figure 5a,c, noted as samples b and c, respectively) at 500 °C within 240 min are shown in Figure 10. For samples a and b, whose BET surface areas are almost the same (56.0 and 59.9 m^2/g, respectively), the C_3H_8 conversion of sample b is much higher than that of sample a. Even for sample c, whose BET surface area (7.1 m^2/g) is much smaller, a relatively higher C_3H_8 conversion could be achieved. The selectivity of the reaction is somewhat lowered for both b and c, but the great increase of C_3H_8 conversion can compensate this loss, leading

to an enhanced yield of C_3H_6. This improved catalytic activity should be ascribed to the structural transition from monazite to zircon type, which stabilizes the surface-active sites.[9] However, we also mentioned that the catalytic efficiency of *t*-$LaVO_4$ nanocrystals is a little lower than that of the zircon-type $REVO_4$ (RE = Ce, Pr, ..., Lu) under almost the same measurement conditions.[9] Detailed studies on optimization of the catalytic efficiency of *t*-$LaVO_4$ will be conducted in the future.

Conclusion

In conclusion, pure monoclinic and tetragonal $LaVO_4$ nanocrystals are obtained by the hydrothermal method. The transition from stable *m*-$LaVO_4$ to metastable *t*-$LaVO_4$ induced by chelating ligands such as EDTA is investigated. The results showed that *t*-$LaVO_4$ could be obtained by the mediation of only a small amount of Na_2H_2L. The steric hindrance effect of EDTA that coordinated with La^{3+} makes it stabilized with fewer coordination sites, and this is proposed as the main reason for the formation of *t*-$LaVO_4$ and the driving force of polymorph transformation from *m*- to *t*-$LaVO_4$. The varied capability of inducing the formation of *t*-$LaVO_4$ by EDTA at different pH values arises from the different coordination ability of EDTA and La^{3+}. Careful investigations over the phase transition process (*t* to *m* transition) were also conducted, revealing enhanced thermal stability of the nanosized metastable *t*-$LaVO_4$ compared with bulk materials due to the small size effect. Our capability of obtaining and stabilizing metastable *t*-$LaVO_4$ not only favors the wider applications of $LaVO_4$ due to its improved catalytic and luminescent performance but also represents a new idea in the studies of polymorph control and selective synthesis of inorganic material.

Acknowledgment. We thank Professor Z. M. Liu and Dr. H. Wang (Dalian Institute of Chemical Physics, CAS) for the measurement of catalytic activity. This work was supported by NSFC (10374006, 20221101, and 20423005) and Founder Foundation of PKU.

Supporting Information Available: XRD patterns of the $LaVO_4$ nanocrystals (summarized in Table 1) obtained at different temperature and pH conditions, luminescence spectra of commercial Y_2O_3−Eu (5%) phosphor, and comparison to *m*- and *t*-$LaVO_4$−Eu (5%) nanocrystals (PDF). This material is available free of charge via the Internet at http://pubs.acs.org.

References and Notes

(1) Huang, W. P.; Tang, X. H.; Wang, Y. Q.; Koltypin, Y.; Gedanken, A. *Chem. Commun*. **2000**, 1415.
(2) Lu, J.; Oi, P. F.; Peng, Y. Y.; Meng, Z. Y.; Yang, Z. P.; Yu, W. C.; Qian, Y. T. *Chem. Mater*. **2001**, *13*, 2169.
(3) Wang, X.; Li, Y. D. *J. Am. Chem. Soc*. **2002**, *124*, 2880.
(4) Wang, X.; Li, Y. D. *Chem.-Eur. J*. **2003**, *9*, 300.
(5) Chen, X. J.; Xu, H. F.; Xu, N. S.; Zhao, F. H.; Lin, W. J.; Lin, G.; Fu, Y. L.; Huang, Z. L.; Wang, H. Z.; Wu, M. M. *Inorg. Chem*. **2003**, *42*, 3100.
(6) Blagden, N.; Davey, R. J. *Cryst. Growth Des*. **2003**, *3*, 873.
(7) Joo, J.; Yu, T.; Kim, Y. W.; Park, H. M.; Wu, F. X.; Zhang, J. Z.; Hyeon, T. *J. Am. Chem. Soc*. **2003**, *125*, 6553.
(8) Lai, J. R.; Shafi, K. V. P. M.; Loos, K.; Ulman, A.; Lee, Y.; Vogt, T.; Estournes, C.; *J. Am. Chem. Soc*. **2003**, *125*, 11470.
(9) Fang, Z. M.; Hong, Q.; Zhou, Z. H.; Dai, S. J.; Weng, W. Z.; Wan, H. L. *Catal. Lett*. **1999**, *61*, 39.
(10) Ross, M. *IEEE J. Quantum Electron*. **1975**, *11*, 938.
(11) O'Connor, J. R. *Appl. Phys. Lett*. **1966**, *9*, 407.
(12) Levine, A. K.; Palilla, F. C. *Appl. Phys. Lett*. **1964**, *5*, 118.
(13) Palilla, F. C.; Levine, A. K.; Rinkevics, M. J. *J. Electrochem. Soc*. **1965**, *112*, 776.
(14) Rambabu, U.; Amalnerkar, D. P.; Kale, B. B.; Buddhudu, S. *Mater. Res. Bull*. **2000**, *35*, 929.
(15) Jia, C. J.; Sun, L. D.; Luo, F.; Jiang, X. C.; Wei, L. H.; Yan, C. H. *Appl. Phys. Lett*. **2004**, *84*, 5305.
(16) Schwarz, H. *Z. Anorg. Allg. Chem*. **1963**, *323*, 44.
(17) Ropp, R. C.; Carroll, B. *J. Inorg. Nucl. Chem*. **1973**, *35*, 1153.
(18) Escobar, M. E.; Baran, E. J. *Z. Anorg. Allg. Chem*. **1978**, *114*, 273.
(19) Chakoumakos, B. C.; Abraham, M. M.; Boatner, L. A. *J. Solid State Chem*. **1994**, *109*, 197.
(20) Oka, Y.; Yao, T.; Yamamoto, N. *J. Solid State Chem*. **2000**, *152*, 486.
(21) Riwotzki, K.; Haase, M. *J. Phys. Chem. B* **1998**, *102*, 10129.
(22) Haase, M.; Riwotzki, K.; Meyssamy, H.; Kornowski, A. *J. Alloy Compd*. **2000**, *303*, 191.
(23) Riwotzki, K.; Haase, M. *J. Phys. Chem. B* **2001**, *105*, 12709.
(24) Huignard, A.; Gacoin, T.; Boilot, J. P. *Chem. Mater*. **2000**, *12*, 1090.
(25) Huignard, A.; Buissette, V.; Laurent, G.; Gacoin, T.; Boilot, J. P. *Chem. Mater*. **2002**, *14*, 2264.
(26) Huignard, A.; Buissette, V.; Franville, A. C.; Gacoin, T.; Boilot, J. P. *J. Phys. Chem. B* **2003**, *107*, 6754.
(27) Sun, L. D.; Zhang, Y. X.; Zhang, J.; Yan, C. H.; Liao, C. S.; Lu, Y. Q. *Solid State Commun*. **2002**, *124*, 35.
(28) Yan, C. H.; Sun, L. D.; Liao, C. S.; Zhang, Y. X.; Lu, Y. Q.; Huang, S. H.; Lu, S. Z. *Appl. Phys. Lett*. **2003**, *82*, 3511.
(29) Wu, H.; Xu, H. F.; Su, Q.; Chen, T. H.; Wu, M. M. *J. Mater. Chem*. **2003**, *13*, 1223.
(30) Zaremba, C. M.; Belcher, A. M.; Fritz, M.; Li, Y. L.; Mann, S.; Hansma, P. K.; Morse, D. E.; Speck, J. S.; Stucky, G. D. *Chem. Mater*. **1996**, *8*, 679.
(31) Cölfen, H.; Antonietti, M. *Langmuir* **1998**, *14*, 582.
(32) Cölfen, H.; Mann, S. *Angew. Chem., Int. Ed*. **2003**, *42*, 2350.
(33) Jiang, X. C.; Sun, L. D.; Feng, W.; Yan, C. H. *Cryst. Growth Des*. **2004**, *4*, 517.
(34) Uchida, M.; Sue, A.; Yoshioka, T.; Okuwaki, A. *CrystEngComm* **2001**, *5*, 1.
(35) Garvie, R. C. *J. Phys. Chem*. **1965**, *69*, 1238.
(36) McHale, J.; Auroux, A.; Perrotta, A.; Navrotsky, A. *Science* **1997**, *277*, 788.
(37) Nuth, J. A. *Nature* **1987**, *329*, 589.
(38) Falini, G.; Albeck, S.; Weiner, S.; Addadi, L. *Science* **1996**, *271*, 67.
(39) Belcher, A. M.; Wu, X. H.; Christensen, R. J.; Hansma, P. K.; Stucky, G. D.; Morse, D. E. *Nature* **1996**, *381*, 56.
(40) López-Macipe, A.; Gómez-Morales, J.; Rodríguez-Clemente, R. *J. Cryst. Growth* **1996**, *166*, 1015.
(41) Peng, Q.; Dong, Y. J.; Deng, Z. X.; Li, Y. D. *Inorg. Chem*. **2002**, *41*, 5249.
(42) Davey, R. J.; Cardew, P. T.; McEwan, D.; Sadler, D. E. *J. Cryst. Growth* **1986**, *79*, 648.
(43) Li, C. M.; Botsaris, G. D.; Kaplan, D. L. *Cryst. Growth Des*. **2002**, *2*, 387.
(44) Seo, S. Y.; Sohn, K. S.; Park, H. D.; Lee, S. *J. Electrochem. Soc*. **2002**, *149*, H12.
(45) Sun, L. D.; Liao, C. S.; Yan, C. H. *J. Solid State Chem*. **2003**, *171*, 304.